

Localization in OFDM Passive Distributed Antenna Systems with Pilots and Unknown Data Payloads: A Marginal Maximum Likelihood Approach

Mathieu Reniers[✉], Martin Willame[✉], Jérôme Louveaux[✉], Luc Vandendorpe[✉],
ICTEAM, UCLouvain - Louvain-La-Neuve, Belgium. Emails: {firstname.lastname}@uclouvain.be

Abstract—Integrated Sensing and Communications (ISAC) is emerging as a key paradigm for future Sixth-Generation (6G) networks, with communication-centric designs favored for their compatibility with existing standards. Communication signals contain both known deterministic pilot symbols and unknown random data payloads. Most localization approaches rely solely on pilots, discarding the position information contained in the data symbols, which constitute the majority of each transmitted frame. Alternatively, Decision-Directed (DD) approaches exploit data decisions, thereby inherently limiting positioning performance to that of the communication system. In this paper, we derive a Marginal Maximum Likelihood (MML) estimator that jointly leverages pilot and data payloads without requiring data decoding, enabling operation with high-order constellations and under challenging noise conditions. We consider an opportunistic scenario in which an Orthogonal Frequency-Division Multiplexing (OFDM) signal transmitted by a User Equipment (UE) is captured by a distributed receiver array. Through numerical simulations, we demonstrate that the proposed method achieves superior localization performance compared to existing approaches and consistently converges to the genie bound (where data symbols are assumed perfectly known) at a lower Signal-to-Noise Ratio (SNR) than any DD method. Furthermore, the proposed method remains robust to constellation size, unlike DD approaches, whose performance degrades with increasing modulation order. Finally, we provide a computational complexity analysis of the proposed method and the considered baselines, highlighting the impact of system parameters on their respective computational costs.

Index Terms—Integrated Sensing and Communication, Non-Data-Aided, Marginal Maximum Likelihood, Data Payloads, Nuisance Parameter, OFDM Passive Radar, Localization

I. INTRODUCTION

INTEGRATED Sensing and Communications (ISAC) is likely to become a cornerstone of future Sixth Generation (6G) networks and next-generation Wi-Fi standards, enabling mobile systems to sense their environment [1]–[3]. Integrating communication and sensing into a single platform allows hardware sharing, improving spectrum efficiency [4] and reducing device cost, size, and power consumption, while potentially enhancing the performance of both services [5], [6]. The *communication-centric* approach—where communication remains the primary function and sensing or radar capabilities are performed by reusing the communication waveform—has emerged as the most promising, owing to its compatibility with existing wireless standards [7]. In this paradigm, the

transmitted communication signal comprises pilot symbols, which are **deterministic** and **known** to both transmitter (TX) and receiver (RX), alongside data symbols, which carry information and are **random** and **unknown** at the RX.

A. Related Works

1) *Pilot-Only Localization*: The traditional approach for ISAC radar sensing relies solely on pilot or reference signals dedicated to this purpose [8]–[10]. Wei et al. [8] investigate radar sensing performance using Fifth Generation New Radio (5G-NR) Positioning Reference Signal (PRS). This work was extended to irregular PRS resource patterns for high-mobility scenarios in [9] and to collaborative multi-reference-signal schemes in [10]. However, these approaches completely overlook the localization information contained in the data payloads, which constitute the majority of each transmitted frame (typically 75%–97% in 5G-NR [11]).

2) *Characterizing Sensing under Random Data Signals*: To address this limitation, several studies instead characterize the sensing performance under random data signals rather than deterministic pilots [12]–[14], typically assuming a monostatic configuration where the sensing receiver (SRX) has perfect knowledge of the transmitted data symbols. Liu et al. [12] show that, among all communication waveforms with cyclic prefix, Orthogonal Frequency-Division Multiplexing (OFDM) is optimal for minimizing ranging sidelobes with Quadrature Amplitude Modulation (QAM), strengthening its candidacy for 6G—and motivating its adoption in this work. Keskin et al. [13] reveal a fundamental *time-frequency trade-off* in monostatic OFDM ISAC: high-order QAM improves communication rates but degrades sensing due to elevated sidelobe levels from the non-constant modulus data [14], whereas low-order Phase-Shift Keying (PSK) minimizes sidelobes at the cost of reduced spectral efficiency. This trade-off has motivated probabilistic constellation shaping approaches aimed at jointly optimizing both functions [14]. While these studies provide valuable insights into the impact of data randomness on sensing, perfect knowledge of the transmitted data at the SRX is not attainable in multistatic nor passive sensing configurations.

3) *Decision-Directed Philosophy*: A natural way to exploit the full transmitted frame is to demodulate the data payloads and treat the decisions as additional pilots, following a Decision-Directed (DD) philosophy. Wypich and Zielinski [15] demonstrate that in OFDM-based passive radar, reconstructed data effectively supplements pilots under low Symbol

Mathieu Reniers is a Research Fellow of the Fonds de la Recherche Scientifique - FNRS.

Error Rate (SER) conditions, while performance reduces to the pilot-only case under challenging channel conditions or high-order modulations—a finding validated experimentally in [16]. Brunner et al. [17] propose a complete bistatic ISAC framework accounting for synchronization and characterize sensing performance over the full frame, including the impact of decoding failures and residual synchronization errors. To enhance sensing performance at a modest spectral efficiency cost, Henninger et al. [18] propose a resource allocation scheme placing lower-order constellation symbols as pseudo-pilots. The DD methodology has also been integrated into iterative frameworks exploiting the mutual benefits of *communication-aided sensing* and *sensing-aided communication* [19], [20]. This approach was first developed for single-carrier bistatic systems by Zhao et al. in [19] and subsequently extended to OFDM by Keskin et al. in [20]. While these methods achieve low localization errors under favorable Signal-to-Noise Ratio (SNR) conditions, they incur high computational complexity due to forward error correction decoding or iterative processing, and their localization performance is inherently limited by that of the communication system.

4) *Maximum Likelihood Philosophy*: An alternative to DD is to treat the unknown data symbols as **Nuisance Parameters (NPs)**, i.e., parameters that affect the distribution of the observations used for estimation but are not of direct interest, as opposed to the **Parameters of Interest (PoIs)**. A natural way to eliminate the dependence on the NPs is to marginalize the likelihood over their prior distribution, i.e., to integrate the conditional likelihood of the observations with respect to the NP prior. This approach is referred to as Marginal Maximum Likelihood (MML), or sometimes as Integrated Maximum Likelihood (IML) in the literature [21]. In the case of data symbols, this amounts to evaluating the conditional likelihood over all constellation points, rather than making hard symbol decisions as in DD. This formulation falls within the class of Non-Data-Aided (NDA) estimation methods, where unknown transmitted symbols are treated as random variables and handled statistically rather than pre-estimated¹. While NDA estimators have been widely studied for communication purposes, their application to positioning remains sparse [24], [25]. Monfared et al. [24] propose an iterative MML-based NDA algorithm using Angle of Arrival measurements for sensor localization with a Gaussian Frequency Shift Keying waveform. Graff and Humphreys [25] derive the MML estimator for OFDM-based positioning, compare pilot-only, DD, and MML range estimation performance against a derived Ziv-Zakai Bound, and apply the framework to simulated low-earth orbit satellite channels. However, their work is limited to a single-antenna receiver where only the data symbols are treated as NPs, while the timing offset, phase offset, and channel gain are either explicitly estimated or assumed known. In contrast, the present work extends this framework to a multi-antenna distributed array operating

¹There is a subtle terminology shift in the recent literature. Originally, NDA refers to estimation using unknown symbols (i.e., data), while Data-Aided (DA) refers to the use of known symbols (i.e., pilots). However, some recent works use DA terminology [20], [22], [23] to describe methods following a DD philosophy.

without phase synchronization, treating the channel coefficient at each antenna as an additional NP, thereby broadening the scope of the MML approach. Furthermore, while their work reports a computational complexity of $\mathcal{O}(\#\mathcal{C})$, where $\#\mathcal{C}$ denotes the constellation size, we introduce an analytical acceleration that reduces it to $\mathcal{O}(\sqrt{\#\mathcal{C}})$.

Another approach to handle NPs is Joint Maximum Likelihood (JML) estimation, where both the PoIs and NPs are *jointly* estimated. In our previous work [26], we applied this method to a source localization scenario restricted to a co-located Uniform Linear Array (ULA) operating under Far-Field (FF) conditions, limitations that the present work overcomes.

B. Contributions

To address the aforementioned limitations, we develop an MML framework for an “uplink”² scenario where the transmitted communication signal from a User Equipment (UE) is captured by an **opportunistic SRX** consisting of **multiple distributed nodes** whose sole objective is to localize the source. Since the nodes are **not phase-synchronized**, the random unknown channel coefficients are treated as additional NPs, alongside the data symbols. Given the distributed nature of the SRX, the spherical nature of the wavefront can no longer be ignored. Our main contributions are summarized as follows:

- We develop the MML framework for uplink localization with a distributed, non-phase-synchronized SRX, treating both data symbols and channel coefficients at all nodes as NPs. The optimal solution is derived and shown to be computationally intractable, motivating the development of practical approximations.
- We propose a computationally feasible approximation of the MML solution. Through Monte Carlo (MC) simulations, we demonstrate superior localization performance over existing methods, with two key findings: the **proposed method is robust to constellation size**—unlike DD methods, whose performance degrades with increasing modulation order—and **converges to the GENIE bound** (i.e., data assumed perfectly known at the SRX) **at lower SNR than competing DD approaches**.
- Additionally, we derive a closed-form computational acceleration of the proposed method for M -QAM constellations, reducing the complexity from $\mathcal{O}(M)$ to $\mathcal{O}(\sqrt{M})$ while yielding the exact same solution. This acceleration is applicable to other likelihood-based problems and, to the best of the authors’ knowledge, has not been previously reported in the literature.
- We provide a comprehensive analysis of the proposed method against the considered baselines, examining the impact of system parameters on both localization performance and computational requirements, supported by theoretical insights and simulation results.

²This terminology is used by analogy with the conventional communication uplink, and is used here interchangeably with source localization.

C. Structure of the Paper

The remainder of the paper is organized as follows. Section II describes the system model, including the scenario, channel model, and signal definitions. In Section III, we derive the optimal MML estimator, establish its computational intractability, introduce a feasible approximation, and present the analytical acceleration for QAM constellations. Section IV presents the MC simulation results and investigates the impact of system parameters on localization performance, as well as the impact of data demodulation errors on DD-based localization. Section V provides a detailed complexity analysis. Finally, Section VI concludes the paper and outlines directions for future work. Throughout this paper, some key observations and discussions are presented in **Remark** environments for ease of reference.

D. Notations

Scalars, vectors, matrices and tensors are respectively denoted by a , \mathbf{a} , \mathbf{A} and \mathcal{A} , and when expressed as function of parameters, written as $a(\cdot)$, $\mathbf{a}(\cdot)$, $\mathbf{A}(\cdot)$ and $\mathcal{A}(\cdot)$. The i -th element of \mathbf{a} , the (i, j) -th element of \mathbf{A} and the (i, j, k) -th element of \mathcal{A} are expressed as $\mathbf{a}[i]$, $\mathbf{A}[i, j]$ and $\mathcal{A}[i, j, k]$. The absolute value, the vector ℓ_2 norm and the Frobenius norm are denoted by $|a|$, $\|\mathbf{a}\|_2$ and $\|\mathbf{A}\|_F$, respectively. The $K \times K$ identity matrix is written as \mathbf{I}_K . The real and complex sets are denoted by \mathbb{R} and \mathbb{C} , the complex conjugate is defined by a^* , and $j \triangleq \sqrt{-1}$. The cardinality of a finite set \mathcal{S} is given by $\#\mathcal{S}$. The likelihood function is represented by $\mathcal{L}(\cdot)$. Given a true quantity θ , candidate and final estimates are indicated by $\hat{\theta}$ and $\hat{\theta}$, respectively. Finally, the expectation over θ is notated $\mathbb{E}_\theta\{\cdot\}$.

II. SYSTEM MODEL

A. Scenario

This paper investigates the problem of localizing a single-antenna UE at position $\mathbf{x}_s \in \mathbb{R}^2$, transmitting an OFDM uplink signal received by an SRX consisting of N single-antenna RX nodes at positions $\{\mathbf{x}_n\}_{n=0}^{N-1} \in \mathbb{R}^{N \times 2}$ and forming a Distributed Antenna System (DAS). Note that the proposed framework can be straightforwardly extended to \mathbb{R}^3 without loss of generality. An illustration of the scenario is presented in Figure 1. Note that the node positions $\{\mathbf{x}_n\}_{n=0}^{N-1}$ are known to the Central Processing Unit (CPU), which estimates \mathbf{x}_s .

The UE transmits P pilot and D data OFDM symbols across Q subcarriers, with a subcarrier spacing of Δ_f , yielding a total bandwidth of $B \triangleq Q\Delta_f$. The frequency corresponding to the first subcarrier is denoted by f_s , with associated wavelength λ_s and wavenumber $k_s \triangleq 2\pi f_s/c = 2\pi/\lambda_s$, where c represents the speed of light. Pilot symbols are given by $\mathcal{S}_P \in \mathbb{C}^{Q \times P}$ and may consist of arbitrary complex sequences. Data symbols are given by $\mathcal{S}_D \in \mathbb{C}^{Q \times D} \subset \mathbb{C}^{Q \times D}$, where each element $\mathcal{S}_D[q, d]$ belongs to a given constellation $\mathcal{C}_{\nu(q, d)} \in \mathcal{C}$, selected from the set \mathcal{C} . The constellation assignment across frequency and time dimensions is denoted by $\nu(q, d)$ and is determined by the TX. It is typically defined in the preamble containing transmission metadata. To simplify notation, we adopt the following shorthand: $\mathcal{S}_D \in \mathcal{C}_\nu^{Q \times D} \triangleq \{\mathcal{S}_D[q, d] \in \mathcal{C}_{\nu(q, d)}\}_{q, d=0}^{Q-1, D-1}$. The symbol

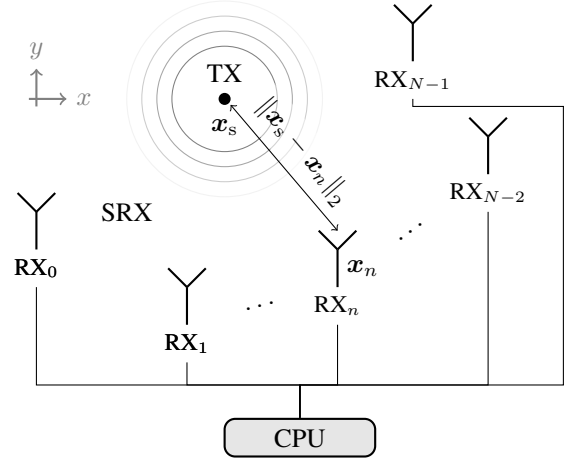


Fig. 1. Illustration of the considered scenario. The UE (i.e., the TX) transmits an uplink signal to a DAS (i.e., the SRX) consisting of N single-antenna RX nodes. A CPU collects the received signals and performs localization.

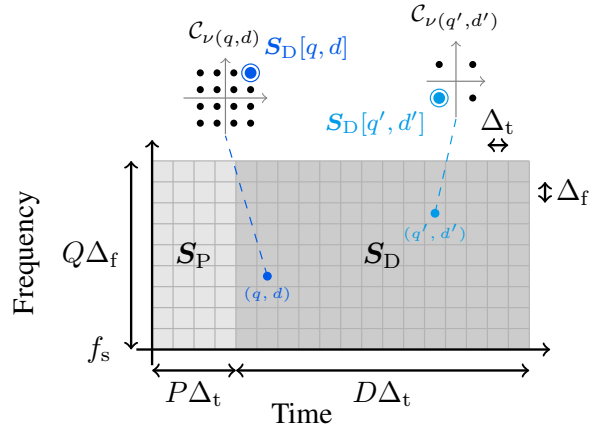


Fig. 2. Illustration of the considered resource grid.

transmission follows the resource grid illustrated in Figure 2. Note that other resource allocations can be accommodated; specifically, the time-domain distribution of pilot and data symbols has no impact, as the channel is assumed constant across the time dimension (see Section II-B), whereas a uniform allocation across the frequency axis is required.

The following assumption is adopted for the considered scenario:

Assumption 1. *The UE and the background are assumed to be stationary during the frame duration $T \triangleq (P+D)\Delta_t$, with Δ_t being the OFDM symbol duration. Hence, no Doppler effect is considered.*

For the typical 6G ISAC parameters used in the simulations (see Table I), this yields³ $\Delta_t \approx \Delta_f^{-1} = 16.67\mu\text{s}$ and $T = (P+D)\Delta_t \approx 0.6\text{ms}$, which is sufficiently short to justify the stationarity assumption over a single localization update.

³Neglecting the cyclic prefix (of length L_{cp}), from $\Delta_t = \frac{Q+L_{cp}}{Q\Delta_f} \approx \Delta_f^{-1}$ for $Q \gg L_{cp}$.

B. Channel model and observations

The channel model is specified under the following assumptions:

Assumption 2. *Only Line of Sight (LoS) propagation is considered.*

Assumption 3. *Time synchronization is already achieved at each RX node, and local oscillators are matched (i.e., no carrier frequency offset) between the UE and all RX nodes.*

The channel matrix is defined as $\mathbf{H}(\mathbf{x}_s) \in \mathbb{C}^{N \times Q}$. Following the aforementioned assumptions, the channel coefficient at the n -th RX node and on the q -th subcarrier can be written as (see, for instance, [27])

$$\mathbf{H}(\mathbf{x}_s)[n, q] = \beta[n] e^{-j2\pi(f_s + q\Delta_f)\|\mathbf{x}_s - \mathbf{x}_n\|_2/c} \quad (1)$$

$$= \underbrace{\beta[n] e^{-jk_s\|\mathbf{x}_s - \mathbf{x}_n\|_2}}_{\triangleq \gamma[n]} \underbrace{e^{-jk_s\|\mathbf{x}_s - \mathbf{x}_n\|_2 q \frac{\Delta_f}{f_s}}}_{\triangleq \mathbf{A}(\mathbf{x}_s)[n, q]}, \quad (2)$$

where $\beta \in \mathbb{C}^{N \times 1}$ contains the random channel coefficient at all nodes, accounting for propagation losses and random phases at each RX; $\gamma \in \mathbb{C}^{N \times 1}$ additionally includes the propagation phases associated with the reference frequency; and $\mathbf{A}(\mathbf{x}_s) \in \mathbb{C}^{N \times Q}$ denotes the steering matrix (i.e., the part of the model that carries the localization information).

Remark II.1. *We consider a distributed SRX operating without phase synchronization, such that each node n exhibits an independent random phase, which is absorbed into $\beta[n]$. Although phase synchronization of distributed arrays has been studied in the literature [28], [29], the opportunistic SRX considered here is assumed to lack the required infrastructure, rendering phase calibration impractical or prohibitively costly due to the associated iterative procedures.*

Remark II.2. *This model assumes that β and therefore γ are constants across the time and frequency domains, which requires $T < T_c$ and $B < B_c$, where T_c and B_c are the coherence time and bandwidth. These conditions are directly satisfied by Assumptions 1 and 2.*

At the SRX, the observations associated with pilot and data components are respectively denoted as $\mathbf{Y}_P \in \mathbb{C}^{N \times Q \times P}$ and $\mathbf{Y}_D \in \mathbb{C}^{N \times Q \times D}$ and are expressed as

$$\mathbf{Y}_P[n, q, p] = \mathbf{H}(\mathbf{x}_s)[n, q] \mathbf{S}_P[q, p] + \mathcal{N}_P[n, q, p], \quad (3)$$

$$\mathbf{Y}_D[n, q, d] = \mathbf{H}(\mathbf{x}_s)[n, q] \mathbf{S}_D[q, d] + \mathcal{N}_D[n, q, d], \quad (4)$$

where $\mathcal{N}_P \in \mathbb{C}^{N \times Q \times P}$ and $\mathcal{N}_D \in \mathbb{C}^{N \times Q \times D}$ are the Additive White Gaussian Noise (AWGN) terms that are independent across all dimensions, with each element following a complex normal distribution $\mathcal{CN}(0, \sigma_n^2)$.

III. MARGINAL MAXIMUM LIKELIHOOD ESTIMATOR

The objective is to estimate the PoI (i.e., the UE position \mathbf{x}_s), from both the pilot and data observations. Since data symbols \mathbf{S}_D are unknown at the SRX, they act as NP, along with channel coefficients γ . To extract position information from \mathbf{Y}_P and \mathbf{Y}_D , one must eliminate the dependence on these NPs. In this paper, we investigate an MML approach,

where NPs uncertainty is eliminated by marginalizing the conditional likelihood over their prior distributions.

The MML estimation problem is expressed as

$$\hat{\mathbf{x}}_s^{\text{MML}} = \underset{\tilde{\mathbf{x}}_s}{\operatorname{argmax}} \mathbb{E}_{\mathbf{S}_D, \gamma} \{ \mathcal{L}(\mathbf{Y}_P, \mathbf{Y}_D | \mathbf{S}_D, \gamma; \tilde{\mathbf{x}}_s) \} \quad (5)$$

$$= \underset{\tilde{\mathbf{x}}_s}{\operatorname{argmax}} \mathbb{E}_{\mathbf{S}_D} \left\{ \underbrace{\mathbb{E}_{\gamma} \{ \mathcal{L}(\mathbf{Y}_P, \mathbf{Y}_D | \mathbf{S}_D, \gamma; \tilde{\mathbf{x}}_s) \}}_{=\mathcal{L}(\mathbf{Y}_P, \mathbf{Y}_D | \mathbf{S}_D; \tilde{\mathbf{x}}_s)} \right\}, \quad (6)$$

$$= \mathcal{L}(\mathbf{Y}_P, \mathbf{Y}_D; \tilde{\mathbf{x}}_s)$$

where $\mathcal{L}(\mathbf{Y}_P, \mathbf{Y}_D | \mathbf{S}_D, \gamma; \tilde{\mathbf{x}}_s)$ denotes the likelihood or probability of observing $(\mathbf{Y}_P, \mathbf{Y}_D)$ conditioned on the **stochastic** NPs (\mathbf{S}_D, γ) and given the *candidate* PoI $\tilde{\mathbf{x}}_s$. Equation (6) follows from the law of total expectation. For brevity, we introduce the time-concatenated quantities $\mathbf{S} \in \mathbb{C}^{Q \times L}$ and $\mathbf{Y} \in \mathbb{C}^{N \times Q \times L}$, where $L \triangleq P + D$ is the total number of OFDM symbols.

This section first derives the optimal solution to (6) by successively marginalizing over γ and \mathbf{S}_D , and shows that it is computationally intractable. A tractable approximation is then derived by leveraging pilot information to eliminate the channel dependency in the data component. Finally, an analytical acceleration is developed for QAM constellations, reducing the computational complexity without any additional approximation.

A. Optimal MML solution

Marginalizing over γ and \mathbf{S}_D in (6) yields the following closed-form expression.

Proposition III.1. *We assume independent and identically distributed (i.i.d.) channel coefficients γ , each following a circularly symmetric complex Gaussian distribution with variance σ_γ^2 , i.e., $\gamma \sim \mathcal{CN}(\mathbf{0}, \sigma_\gamma^2 \mathbf{I}_N)$, and data symbols drawn independently and uniformly from their respective constellations, i.e., $\forall q, d \mathbf{S}_D[q, d] \sim \mathcal{U}_{\mathcal{C}_{\nu(q,d)}}$. Marginalizing out γ and \mathbf{S}_D in (6) then yields*

$$\hat{\mathbf{x}}_s^{\text{MML}} = \underset{\tilde{\mathbf{x}}_s}{\operatorname{argmax}} \sum_{\mathbf{S}_D \in \mathbb{C}^{Q \times D}} \mathcal{L}(\mathbf{Y} | \mathbf{S}_D; \tilde{\mathbf{x}}_s) \mathcal{L}(\mathbf{S}_D), \quad (7)$$

where the conditional likelihood is given by

$$\mathcal{L}(\mathbf{Y} | \mathbf{S}_D; \tilde{\mathbf{x}}_s) = C \left(\frac{1}{\sigma_n^2} \sum_{q,l} |\mathbf{S}[q, l]|^2 + \frac{1}{\sigma_\gamma^2} \right)^{-N}$$

$$\times \exp \left(\frac{\sum_n \left| \frac{1}{\sigma_n^2} \sum_{q,l} \mathbf{Y}^*[n, q, l] \mathbf{A}(\tilde{\mathbf{x}}_s)[n, q] \mathbf{S}[q, l] \right|^2}{\frac{1}{\sigma_n^2} \sum_{q,l} |\mathbf{S}[q, l]|^2 + \frac{1}{\sigma_\gamma^2}} \right), \quad (8)$$

and $C \in \mathbb{R}$ is a constant whose expression is provided in Appendix A

Proof. See Appendix A. \square

Remark III.1. *Proposition III.1 reveals that spatial coherence across receivers (n) is lost when marginalizing over the channel coefficients γ . Indeed, due to the distributed nature of the array, each node n experiences an independent random complex coefficient $\beta[n]$, so that the received signals are no longer phase-aligned across space. As a result, the contributions of different receivers combine incoherently, which is reflected in (8) by the summation over receiver indices outside the squared norm. This loss of spatial coherence **degrades the likelihood function**, as will be discussed in Section IV-E (see Figure 10). In contrast, frequency (q) and time (l) coherence are preserved, as the expression remains conditioned on \mathbf{S}_D and all receivers share the same transmitted symbol sequence.*

Note that the resulting estimator requires knowledge of the noise variance σ_n^2 , which in practice can be estimated from the SNR using various existing techniques [30]–[32].

Remark III.2. *Due to the discrete nature of the data symbols and the preservation of time and frequency coherence, the MML estimator in (7) requires an exhaustive evaluation over all possible symbol combinations $\mathbf{S}_D \in \mathcal{C}_\nu^{Q \times D}$. This involves $\mathcal{O}(M_{\max}^{QD})$ combinations, where $M_{\max} \triangleq \max_{q,d} \#\mathcal{C}_{\nu(q,d)}$ is the largest constellation size. Even for a modest configuration with $D = 4$, $Q = 8$, and 16-QAM, this amounts to $16^{8 \times 4} \approx 3.4 \times 10^{38}$ combinations—far beyond any practical computational capability. This exponential complexity renders the optimal MML estimator computationally intractable in practice.*

B. Approximate MML solution

To enable a tractable solution, we introduce an approximation of the MML estimator. The approximation consists of eliminating the dependency on the channel coefficients γ in the data term by substituting a pilot-based estimate constructed for a candidate position $\tilde{\mathbf{x}}_s$, denoted $\hat{\gamma}_p(\tilde{\mathbf{x}}_s)$. The resulting approximate MML estimator is given by

$$\begin{aligned} \hat{\mathbf{x}}_s^{\text{MML}_a} &= \underset{\tilde{\mathbf{x}}_s}{\operatorname{argmax}} \mathbb{E}_{\mathbf{S}_D, \gamma} \left\{ \mathcal{L}(\mathcal{Y}_P | \gamma; \tilde{\mathbf{x}}_s) \right. \\ &\quad \left. \times \mathcal{L}(\mathcal{Y}_D | \mathbf{S}_D; \tilde{\mathbf{x}}_s, \hat{\gamma}_p(\tilde{\mathbf{x}}_s)) \right\} \quad (9) \\ &= \underset{\tilde{\mathbf{x}}_s}{\operatorname{argmax}} \underbrace{\mathbb{E}_\gamma \left\{ \mathcal{L}(\mathcal{Y}_P | \gamma; \tilde{\mathbf{x}}_s) \right\}}_{\text{Pilot term}} \\ &\quad \times \underbrace{\mathbb{E}_{\mathbf{S}_D} \left\{ \mathcal{L}(\mathcal{Y}_D | \mathbf{S}_D; \tilde{\mathbf{x}}_s, \hat{\gamma}_p(\tilde{\mathbf{x}}_s)) \right\}}_{\text{Data term}}, \quad (10) \end{aligned}$$

where (9) follows from (6) by injecting the approximation $\mathcal{L}(\mathcal{Y}_D | \gamma, \mathbf{S}_D; \tilde{\mathbf{x}}_s) \approx \mathcal{L}(\mathcal{Y}_D | \mathbf{S}_D; \tilde{\mathbf{x}}_s, \hat{\gamma}_p(\tilde{\mathbf{x}}_s))$. This approximation eliminates the NP γ dependency through the pilot term, while the \mathbf{S}_D dependency is handled by marginalization in the data term. Indeed, the data term now depends on a single NP term, for which this marginalization can be computed efficiently, as highlighted in Remark III.4. The pilot-based channel coefficient estimate is obtained from

$$\hat{\gamma}_p(\tilde{\mathbf{x}}_s) = \underset{\tilde{\gamma} \in \mathbb{C}^{N \times 1}}{\operatorname{argmax}} \mathcal{L}(\mathcal{Y}_P; \tilde{\gamma}, \tilde{\mathbf{x}}_s), \quad (11)$$

which is separable across receivers n . Applying Wirtinger calculus [33] yields

$$\hat{\gamma}_p(\tilde{\mathbf{x}}_s)[n] = \frac{\sum_{q,p=0,0}^{Q-1,P-1} \mathbf{A}^*(\tilde{\mathbf{x}}_s)[n,q] \mathbf{S}_P^*[q,p] \mathcal{Y}_P[n,q,p]}{\sum_{q,p=0,0}^{Q-1,P-1} |\mathbf{A}(\tilde{\mathbf{x}}_s)[n,q] \mathbf{S}_P[q,p]|^2} \quad (12)$$

$$= \frac{1}{\mathcal{P}_P} \sum_{q=0}^{Q-1} \mathbf{A}^*(\tilde{\mathbf{x}}_s)[n,q] \mathbf{Y}_P[n,q], \quad (13)$$

where the denominator reduces to the pilot energy $\mathcal{P}_P \triangleq \|\mathbf{S}_P\|_F^2$ since $\forall \tilde{\mathbf{x}}_s |\mathbf{A}(\tilde{\mathbf{x}}_s)[n,q]|^2 = 1$, and where the ‘‘symbol-equalized’’ pilot observations $\mathbf{Y}_P \in \mathbb{C}^{N \times Q}$ are defined as

$$\mathbf{Y}_P[n,q] \triangleq \sum_{p=0}^{P-1} \mathbf{S}_P^*[q,p] \mathcal{Y}_P[n,q,p], \quad (14)$$

as this quantity will be useful in the following. For clarity in subsequent expressions, we also define $\widehat{\mathbf{H}}_P(\tilde{\mathbf{x}}_s) \in \mathbb{C}^{N \times Q}$ as the channel estimate constructed for a candidate position $\tilde{\mathbf{x}}_s$, combining the pilot-based estimate of the random coefficient $\gamma[n]$ with the steering matrix defined in (2):

$$\widehat{\mathbf{H}}_P(\tilde{\mathbf{x}}_s)[n,q] = \hat{\gamma}_p(\tilde{\mathbf{x}}_s)[n] \mathbf{A}(\tilde{\mathbf{x}}_s)[n,q]. \quad (15)$$

Proposition III.2. *Assuming the following distributions: $\gamma \sim \mathcal{CN}(\mathbf{0}, \sigma_\gamma^2 \mathbf{I}_N)$ and $\forall q, d \mathbf{S}_D[q,d] \sim \mathcal{U}_{\mathcal{C}_{\nu(q,d)}}$, independently, the estimator $\hat{\mathbf{x}}_s^{\text{MML}_a}$ defined in (10) admits the closed-form expression (16).*

Proof. See Appendix B. \square

Remark III.3. *Similarly to $\hat{\mathbf{x}}_s^{\text{MML}}$, the contributions of different receivers combine incoherently in the pilot term, while in the data term they combine pseudo-coherently. Indeed, the phase correction provided by $\hat{\gamma}_p$ realigns the observations across the spatial dimension. However, since the data symbols differ across subcarriers and time instants, coherence in both frequency and time is lost in the second term. Intuitively, the second term of (16) sums over all possible transmitted symbols on each subcarrier q and time instant d . Ideally, the correct symbol contributes the most when $\tilde{\mathbf{x}}_s = \mathbf{x}_s$, guiding the estimator toward the ground-truth value.*

Remark III.4. *Finally, unlike (7), which requires exhaustively enumerating all possible combinations $\mathbf{S}_D \in \mathcal{C}_\nu^{Q \times D}$, the data term in (16) only requires evaluating all possible constellation points for each (q, d) pair **individually** ($s \in \mathcal{C}_{\nu(q,d)}$), resulting in a tractable computational complexity.*

C. Acceleration for Quadrature Amplitude Modulation

The estimator $\hat{\mathbf{x}}_s^{\text{MML}_a}$ (16) incurs a computational complexity that is linear in M_{\max} , denoted by $\mathcal{O}(M_{\max})$, as one must iterate over all constellation points for each time-frequency sample. In Proposition III.3, we show that when QAM constellations are used, the complexity can be reduced to $\mathcal{O}(\sqrt{M_{\max}})$ while yielding the exact same solution, by analytically reformulating (16). For an M -QAM constellation, the symbols are defined as [11]

$$s_{r,i} = \frac{1}{\sqrt{\mathcal{E}_M}} \left((2r - \sqrt{M} + 1) + (2i - \sqrt{M} + 1)j \right), \quad (17)$$

$$\hat{\mathbf{x}}_s^{\text{MML}_a} = \underset{\tilde{\mathbf{x}}_s}{\operatorname{argmax}} \left(\frac{\mathcal{P}_P}{\sigma_n^2} + \frac{1}{\sigma_\gamma^2} \right)^{-1} \sum_{n=0}^{N-1} \left| \frac{1}{\sigma_n^2} \sum_{q=0}^{Q-1} \mathbf{Y}_P^*[n, q] \mathbf{A}(\tilde{\mathbf{x}}_s)[n, q] \right|^2 + \sum_{q=0}^{Q-1} \sum_{d=0}^{D-1} \log \left(\sum_{s \in \mathcal{C}_{\nu}(q, d)} \exp \left(\frac{2}{\sigma_n^2} \Re \left\{ s \sum_{n=0}^{N-1} \mathcal{Y}_D^*[n, q, d] \widehat{\mathbf{H}}_P(\tilde{\mathbf{x}}_s)[n, q] \right\} - \frac{1}{\sigma_n^2} |s|^2 \sum_{n=0}^{N-1} \left| \widehat{\mathbf{H}}_P(\tilde{\mathbf{x}}_s)[n, q] \right|^2 \right) \right) \quad (16)$$

$$\hat{\mathbf{x}}_s^{\text{MML}_{\text{fast}}} = \underset{\tilde{\mathbf{x}}_s}{\operatorname{argmax}} \left(\frac{\mathcal{P}_P}{\sigma_n^2} + \frac{1}{\sigma_\gamma^2} \right)^{-1} \sum_{n=0}^{N-1} \left| \frac{1}{\sigma_n^2} \sum_{q=0}^{Q-1} \mathbf{Y}_P^*[n, q] \mathbf{A}(\tilde{\mathbf{x}}_s)[n, q] \right|^2 + \sum_{q=0}^{Q-1} \sum_{d=0}^{D-1} \sum_{\mathfrak{F} \in \{\Re, \Im\}} \log \left(\sum_{\substack{k=1 \\ k \text{ odd}}}^{\sqrt{M_{qd}}-1} 2 \cosh \left(\frac{2k}{\sigma_n^2 \sqrt{\mathcal{E}_{M_{qd}}}} \mathfrak{F} \left\{ \sum_{n=0}^{N-1} \mathcal{Y}_D^*[n, q, d] \widehat{\mathbf{H}}_P(\tilde{\mathbf{x}}_s)[n, q] \right\} \right) \exp \left(-\frac{k^2}{\sigma_n^2 \mathcal{E}_{M_{qd}}} \sum_{n=0}^{N-1} \left| \widehat{\mathbf{H}}_P(\tilde{\mathbf{x}}_s)[n, q] \right|^2 \right) \right) \quad (18)$$

for $0 \leq r, i \in \mathbb{Z} \leq \sqrt{M} - 1$, and with $\mathcal{E}_M \triangleq 2(M-1)/3$.

Proposition III.3. *By substituting the explicit expression of the QAM symbols into (16) and grouping terms of similar amplitude along both the real and imaginary axes, the estimator reduces to Equation (18), where $M_{qd} = \#\mathcal{C}_{\nu}(q, d)$.*

Proof. See Appendix C. \square

Remark III.5. *Rather than iterating over all constellation points, $\hat{\mathbf{x}}_s^{\text{MML}_{\text{fast}}}$ (18) only requires two passes over $\sqrt{M_{qd}}/2$ values, separately for the real and imaginary parts. This reduction is achieved by grouping constellation points of equal amplitude, as illustrated in Figure 3, which highlights that a QAM constellation can be decomposed into a set of Binary Phase-Shift Keying (BPSK)-like constellations at increasing amplitude levels along each axis. This structure is also exploited analytically in the proof provided in Appendix C.*

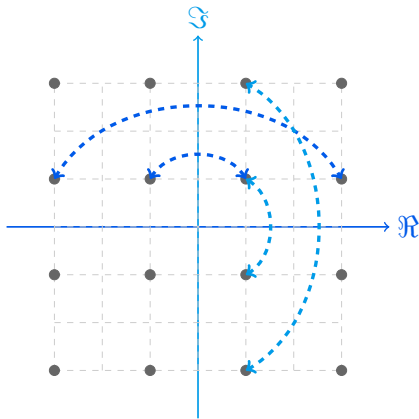


Fig. 3. 16-QAM constellation decomposed into BPSK-like amplitude levels along the real and imaginary axes (indicated by dashed arrows).

Finally, it is worth emphasizing that this reformulation is purely analytical: MML_{fast} (18) is guaranteed to yield **identical position estimates** to MML_a (16), i.e., $\hat{\mathbf{x}}_s^{\text{MML}_{\text{fast}}} = \hat{\mathbf{x}}_s^{\text{MML}_a}$, while achieving significant computational savings, especially for large constellations. Note that a detailed complexity analysis of both variants is presented in Section V.

IV. NUMERICAL RESULTS

This section presents MC simulation results to assess the localization accuracy of the proposed estimator $\hat{\mathbf{x}}_s^{\text{MML}_{\text{fast}}}$ and compare it against existing methods from the literature.

A. Baselines

For all methods, localization is performed in two steps: a **coarse estimate** obtained by searching over a discrete grid of N_g points defined over the scene, followed by a **refinement** using an optimization algorithm (here, the Nelder-Mead method [34]). The following baselines are considered for comparison.

1) **PILOT**: The simplest estimator relies solely on the pilot component, discarding the data part entirely. This is the **traditional approach** employed in current systems, and is obtained by retaining only the first term of (18) and discarding constant coefficients:

$$\hat{\mathbf{x}}_s^{\text{PILOT}} = \underset{\tilde{\mathbf{x}}_s}{\operatorname{argmax}} \sum_{n=0}^{N-1} \left| \underbrace{\sum_{q=0}^{Q-1} \mathbf{Y}_P^*[n, q] \mathbf{A}(\tilde{\mathbf{x}}_s)[n, q]}_{\triangleq \phi_n^P(\tilde{\mathbf{x}}_s)} \right|^2, \quad (19)$$

where $\phi_n^P(\tilde{\mathbf{x}}_s)$ is introduced here for convenience, as it will be reused in the complexity analysis of Section V.

2) **GENIE**: This estimator represents the **best theoretically achievable performance**, obtained by assuming that the data symbols are perfectly known (or perfectly demodulated) at the SRX. In this case, all $P+D$ symbols are treated as pilots by replacing the pilot-equalized observations \mathbf{Y}_P with the full-frame equivalent $\mathbf{Y} \in \mathbb{C}^{N \times Q}$ in (19), defined as

$$\mathbf{Y}[n, q] = \mathbf{Y}_P[n, q] + \sum_{d=0}^{D-1} \mathbf{S}_D^*[q, d] \mathcal{Y}_D[n, q, d]. \quad (20)$$

3) **DECISION-DIRECTED**: In the DD philosophy, the UE position is estimated by using the **data symbol estimates as additional pilots**. This method follows the expression of GENIE, replacing the known \mathbf{S}_D with its estimate, and thus suffers from potential demodulation errors. Since the SRX is distributed, demodulation can be performed in either a *distributed* or *centralized* manner. In the former, each of the

N nodes independently estimates its Q channel coefficients from the pilot observations and performs data demodulation, which yields N potentially different sequences collected in $\widehat{\mathbf{S}}_D \in \mathbb{C}^{N \times Q \times D}$. In the latter, each node forwards its data observations to the CPU, which estimates the channel coefficients and performs centralized data estimation to produce a single sequence $\widehat{\mathbf{S}}_D \in \mathbb{C}^{Q \times D}$. Note that in each approach, both the channel and data estimations are based on the Linear Minimum Mean Square Error (LMMSE) criterion⁴. The *distributed* DD estimator takes the form

$$\widehat{\mathbf{x}}_s^{\text{DD}} = \underset{\widehat{\mathbf{x}}_s}{\operatorname{argmax}} \sum_{n=0}^{N-1} \left| \underbrace{\sum_{q=0}^{Q-1} \mathbf{Y}_{\text{DD}}^*[n, q] \mathbf{A}(\widehat{\mathbf{x}}_s)[n, q]}_{\triangleq \phi_n^{\text{DD}}(\widehat{\mathbf{x}}_s)} \right|^2, \quad \text{with} \quad (21)$$

$$\mathbf{Y}_{\text{DD}}[n, q] \triangleq \mathbf{Y}_P[n, q] + \sum_{d=0}^{D-1} \widehat{\mathbf{S}}_D^*[n, q, d] \mathbf{Y}_D[n, q, d], \quad (22)$$

while the *centralized* variant is obtained by replacing $\widehat{\mathbf{S}}_D[n, q, d]$ with $\widehat{\mathbf{S}}_D[q, d]$ in (22). As before, $\phi_n^{\text{DD}}(\widehat{\mathbf{x}}_s)$ is defined here for reference in Section V. The data estimates can either be mapped to the closest constellation point, referred to as *hard* decisions (Hard-Decision-Directed (HDD)), or left in the complex plane without mapping, referred to as *soft* decisions (Soft-Decision-Directed (SDD)). In the following, observations referring to DD without further specification apply to both HDD and SDD. Note that these DD methods operate directly on symbols without accounting for error-correction coding, as we assume the passive system either lacks access to coding information or prefers to avoid performing such computationally intensive decoding.

B. Simulation Framework and Metrics

To evaluate localization performance, we report the Root Mean Square Error (RMSE) of the position estimate,

$$\text{RMSE}\{\widehat{\mathbf{x}}_s\} = \sqrt{\mathbb{E}\{\|\widehat{\mathbf{x}}_s - \mathbf{x}_s\|_2^2\}}, \quad (23)$$

as a function of the per-node average SNR, defined as

$$\text{SNR} = \frac{\mathbb{E}_{n, \gamma} \left\{ |\gamma[n]|^2 \right\} \sigma_s^2}{\sigma_n^2}, \quad (24)$$

where σ_s^2 is the symbol variance, assumed identical for pilot and data symbols and normalized to $\sigma_s^2 = 1$. Under Assumptions 1 and 2, no fading is considered. Following the physical optics approximation [35], the channel coefficients are modeled in simulation as

$$\beta[n] = e^{j\phi_n} \frac{1}{\|\mathbf{x}_s - \mathbf{x}_n\|_2}, \quad (25)$$

where $\phi_n \sim \mathcal{U}_{[0, 2\pi)}$ accounts for the lack of phase synchronization across nodes.

Additionally, to highlight the interplay between sensing and communication performance, we consider the following communication metrics: the Symbol Error Rate (SER), based on hard decisions, and the Mean Absolute Error (MAE) of the soft data estimates.

⁴A Zero Forcing (ZF)-based estimation was also considered but provides results very similar to, though slightly worse than, the LMMSE-based approach and is therefore not shown here for graph readability.

TABLE I
DEFAULT PARAMETERS USED IN SIMULATION

UE	
Carrier frequency f_s	7.2 GHz
Subcarrier spacing Δ_f	60 kHz
Number of subcarriers Q	128
Number of pilot OFDM symbols P	1
Number of data OFDM symbols D	35
Pilots	BPSK
Data constellation $\mathcal{C}_{\nu(q,d)}$	256-QAM ($\forall q, d$)
SRX	
Number of nodes N	5
Radius R_{SRX}	$5000 \lambda_s = 208.3 \text{ m}$
Aperture θ_{SRX}	$2\pi \text{ rad}$
Simulation	
Scene radius R_{scene}	$4800 \lambda_s = 200 \text{ m}$
Number of grid points N_g (square area of side $2R_{\text{scene}}$)	$40^2 = 1600$
Refinement optimization method	Nelder-Mead [34]
Number of MC iterations N_{mc}	3000

While the developed framework is general and applies to any DAS geometry, we adopt a Uniform Circular Array of radius R_{SRX} and aperture $\theta_{\text{SRX}} \in (0, 2\pi]$ in the simulations. The UE is placed uniformly at random on a disk of radius⁵ $R_{\text{scene}} < R_{\text{SRX}}$. Each node experiences a different attenuation, while σ_n^2 is kept constant across nodes and set from the averaged SNR. The averaged SNR is defined as $\text{SNR} = 2/(R_{\text{scene}}^2 \sigma_n^2)$, which follows from the rough approximation $\mathbb{E}_{n, \gamma} \{ |\gamma[n]|^2 \} = \mathbb{E}_{n, \mathbf{x}_s} \{ \|\mathbf{x}_s - \mathbf{x}_n\|_2^{-2} \} \approx 2/R_{\text{scene}}^2$ in this configuration.

Unless otherwise stated, the simulation parameters are summarized in Table I, where the frequency band used by the UE follows future recommendations for ISAC in 6G [36].

C. Localization Performance

Figures 4 and 5 show the localization RMSE and communication SER, respectively, as a function of SNR for different constellation sizes. The following observations can be drawn:

- As expected, the *distributed* DD methods perform worse than the *centralized* ones, as collaborative demodulation improves the quality of the data symbol estimates (Figure 5) and thus the localization performance (Figure 4), while the potentially different sequences $\widehat{\mathbf{S}}_D$ across nodes in the distributed case degrade the coherence being created in (22).
- Once all data symbols are correctly demodulated, the HDD methods converge to the GENIE performance. In practice, this convergence is observed when $\text{SER} \lesssim 10^{-2}$. As expected, this occurs at higher SNR for larger constellations, due to increased demodulation difficulty.
- The proposed MML_{fast} approach achieves **significant localization improvement over the traditional pilot-only** method, with a reduction in RMSE by a factor of up to 6 across all constellations and under the considered parameter settings (highlighted by \downarrow).

⁵A small margin is introduced to avoid the singularity of the $\|\mathbf{x}_s - \mathbf{x}_n\|_2^{-1}$ path-loss model as $\|\mathbf{x}_s - \mathbf{x}_n\|_2 \rightarrow 0$.

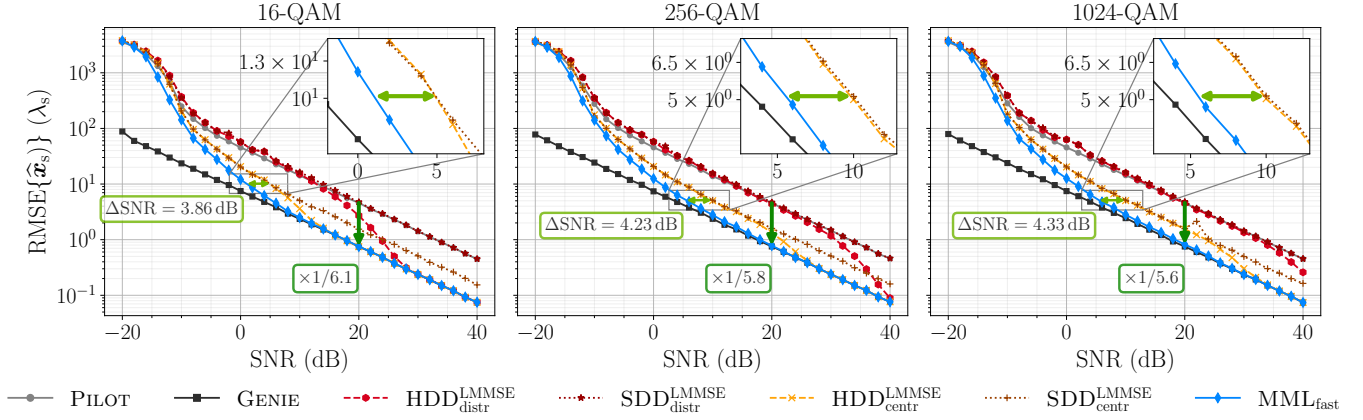


Fig. 4. RMSE as a function of SNR for different data constellations. *Hard* (resp. *soft*) DD baselines are represented by dashed (resp. dotted) lines. The proposed method is shown as a solid blue line with diamond markers, while PILOT and GENIE are shown as solid lines with circle and square markers, respectively. Note that the RMSE is normalized with respect to λ_s (here 4.17 cm).

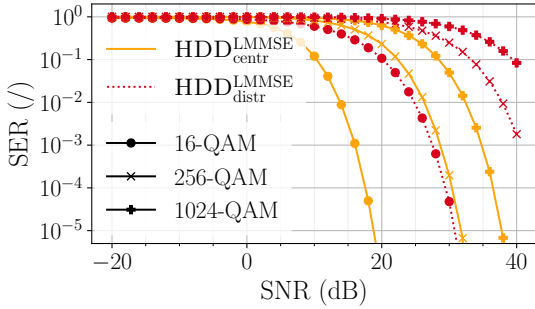


Fig. 5. SER as a function of the SNR, for different data constellations.

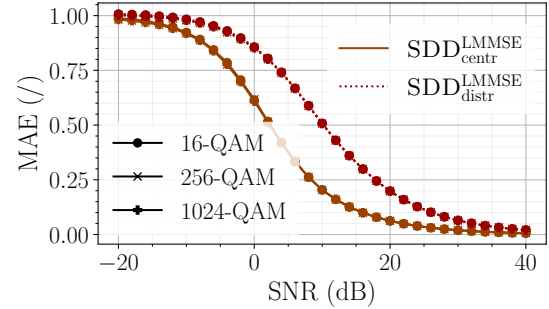


Fig. 6. MAE as a function of the SNR, for different data constellations.

- The proposed MML_{fast} approach **consistently converges to the GENIE bound at lower SNRs than any DD method**, regardless of the constellation. Additionally, while HDD methods suffer from degraded localization performance as the constellation size grows, the proposed approach remains **robust to constellation size**: the increased symbol uncertainty does not result in a noticeable increase in localization error, which is particularly beneficial for high data-rate communications. For the considered set of parameters, SNR improvements of up to 4.3 dB over the best DD baseline are observed (highlighted by \leftrightarrow). Note that this robustness comes at the computational cost of iterating over a larger number of constellation points since M_{qd} increases in (18), as will be discussed in Section V.

D. Impact of Errors on DD Localization

It is also instructive to analyze the effect of symbol errors on the behavior of DD baselines. Comparing the RMSE against the SER, we observe that for the *centralized* HDD, **demodulation errors are less detrimental to localization performance than one might expect**⁶. For instance, for 1024-QAM and $SNR \in [0, 20]$ dB, exploiting the full frame with data decisions significantly improves localization compared to using pilots only (Figure 4), even when the SER remains high (Figure 5), confirming that positioning information is

present even when symbols are not correctly demodulated. This can be attributed to the discrete nature of the SER metric: a soft estimate mapped to an incorrect constellation point is counted as a full symbol error, regardless of how close it lies to the true symbol. This is further corroborated by Figure 6, which shows the MAE of the soft data symbol estimates for the same constellation sizes. The MAE exhibits a significant decrease over $SNR \in [0, 20]$ dB and is, as expected, independent of the constellation size. Consequently, the **MAE (soft estimation) governs the first RMSE drop of HDD_{centr} over PILOT**—consistent across all constellation sizes—while the **SER (constellation mapping) governs the second drop** toward GENIE performance, which occurs at higher SNR for larger constellations. This is further confirmed by the RMSE of the SDD_{centr} method (Figure 4), which benefits only from the first gain⁷. This effect is especially pronounced for large constellations (i.e., a larger SNR gap between the two drops), where a **misclassified symbol** may still lie geometrically **close to the correct one** in the complex plane, and thus **carry substantial positioning information** that contributes beneficially to localization.

⁶A similar observation was reported by Henninger et al. [18] in a different scenario, for a single-antenna receiver producing a single demodulated sequence—analogue to the *centralized* case considered here—further supporting the finding that sensing from data symbols does not require correct decoding of the entire frame.

Finally, HDD methods only close their performance gap with GENIE when data estimation becomes nearly perfect, which occurs at increasingly high SNR for larger constellations. **In contrast, the proposed MML approach closes this gap at significantly lower SNR, consistently across all constellation sizes.**

E. Impact of System Parameters

This section analyzes the impact of system parameters on the localization performance. A summary of the results is provided in Table II.

TABLE II
IMPACT OF SYSTEM PARAMETERS ON LOCALIZATION RMSE.

	PILOT	GENIE	HDD	MML _{fast}	Figure
$\uparrow P$	\downarrow	\downarrow	\downarrow	\downarrow	-
$\uparrow D$	-	\downarrow	\downarrow	\downarrow	7
$\uparrow M_{qd}$	-	-	\uparrow	-	4
$\uparrow N$	$\downarrow\downarrow$	$\downarrow\downarrow$	$\downarrow\downarrow$	$\downarrow\downarrow$	8
$\uparrow Q$	$\downarrow\downarrow$	$\downarrow\downarrow$	$\downarrow\downarrow$	$\downarrow\downarrow$	9

1) *Number of data symbols:* Figure 7 shows the RMSE as a function of D for different SNR values. Increasing D naturally improves the performance of the GENIE bound and benefits HDD methods, although these gains become significant only at SNR values where data estimation is nearly perfect. Similarly, MML_{fast} benefits from additional data observations only when the SNR is sufficiently high for the data symbols to meaningfully guide the estimator toward the true solution (see Remark III.3). At lower SNR, increasing D yields only limited performance gains, as reflected by the saturation behavior observed in the figure. Unlike pilot symbols, which directly reduce the RMSE by increasing the useful signal energy—so that increasing P consistently improves estimation (as observed for GENIE here)—increasing D enhances the performance of MML_{fast} and HDD methods only up to a certain point, beyond which a plateau is reached due to imperfect data estimation. This indicates that the available positioning information becomes limited by the data uncertainty, such that further increases in D provide diminishing returns. Finally, it is worth noting that this regime corresponds to very large D , for which Assumption 1 may no longer hold.

2) *Number of RX nodes:* Figure 8 depicts the RMSE with respect to N for multiple SNR values. Increasing N reduces the RMSE for all methods. For MML_{fast}, this improves both the array (i.e., non-coherent) gain (\sum_n outside the $|\cdot|^2$) of the pilot term and the *pseudo-coherent* combining of the data observations in (18). For centralized HDD approaches, additional nodes lead to better estimation of the data sequence—whose impact on localization has been discussed in Section IV-D—while both centralized and distributed HDD methods benefit from the increased array gain over the combined pilot symbols (i.e., pilots and estimated data symbols treated jointly as $P + D$ pilots, as seen in (22)).

⁷As observed in Figure 4, the *distributed* HDD benefits only from the second gain, while the *distributed* SDD yields no improvement over PILOT across the considered SNR range. This behavior is due to the coherence degradation induced by the potentially differing sequences, as previously discussed.

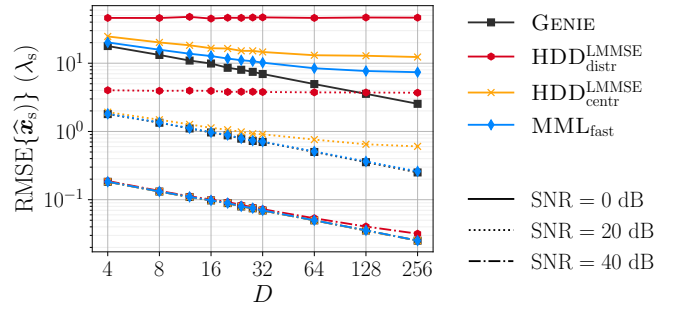


Fig. 7. RMSE as a function of D for different SNR values. Parameters: $N = 8$, $Q = 64$, $\Delta_f = 120$ kHz (yielding the same bandwidth as in Table I), $N_{mc} = 2000$; all other parameters are left at their default values.

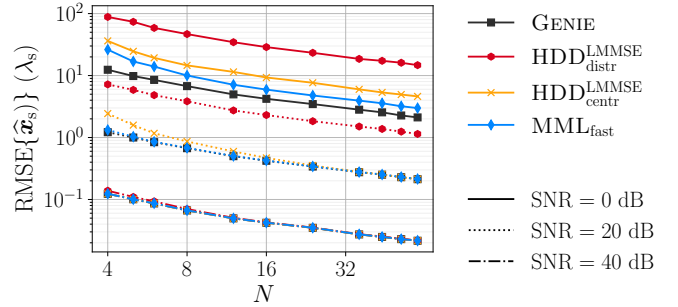


Fig. 8. RMSE as a function of N for different SNR values. Parameters: $Q = 64$, $\Delta_f = 120$ kHz (yielding the same bandwidth as in Table I), $N_{mc} = 2000$; all other parameters are left at their default values.

3) *Number of subcarriers:* Figure 9 represents the RMSE as a function of Q for different SNRs. Increasing Q improves localization for all methods, though the performance gap between methods again depends on the operating SNR, i.e., whether the data observations provide near-perfect positioning information or not. This improvement benefits all methods through the bandwidth coherent gain (\sum_q inside the $|\cdot|^2$) in the pilot term—or combined pilot term for HDD methods—while MML_{fast} additionally benefits from the non-coherent bandwidth gain in the data term of (18). Hence, it is observed that at low SNR, increasing Q benefits the proposed approach more strongly than the HDD baselines.

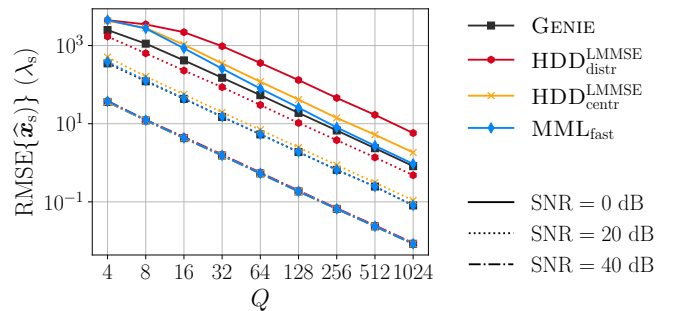


Fig. 9. RMSE as a function of Q for different SNR values. Parameters: $N = 8$, $\Delta_f = 120$ kHz, $N_{mc} = 2000$; all other parameters are left at their default values.

The effect of the bandwidth coherent gain is illustrated in Figure 10, which shows the Ambiguity Function (AF)

for different values of Q for both the space-coherent and non-space-coherent cases, and highlights the intrinsic range resolution $R_{\text{res}} = \frac{c}{2B} = \frac{f_s \lambda_s}{Q \Delta_f}$ (indicated by the double-headed arrows in the figure). These AF functions are defined as

$$\text{AF}_{\text{coh}}(\mathbf{x}_s, \tilde{\mathbf{x}}_s) = \sum_{n=0}^{N-1} \sum_{q=0}^{Q-1} e^{-jk_s(\|\mathbf{x}_s - \mathbf{x}_n\|_2 - \|\tilde{\mathbf{x}}_s - \mathbf{x}_n\|_2)q \frac{\Delta_f}{f_s}}, \quad (26)$$

$$\text{AF}_{\text{non-coh}}(\mathbf{x}_s, \tilde{\mathbf{x}}_s) = \sum_{n=0}^{N-1} \left| \sum_{q=0}^{Q-1} e^{-jk_s(\|\mathbf{x}_s - \mathbf{x}_n\|_2 - \|\tilde{\mathbf{x}}_s - \mathbf{x}_n\|_2)q \frac{\Delta_f}{f_s}} \right|^2, \quad (27)$$

where the attenuation term is omitted since the localization procedure does not exploit this information. These functions correspond to the noise-free output of a filter matched to the candidate position $\tilde{\mathbf{x}}_s$ for a source located at \mathbf{x}_s [37], following a Maximum Likelihood (ML) approach in the presence of AWGN. In particular, the non-coherent AF directly corresponds to the noise-free log-likelihood of the pilot-only estimator (19) when $P = 1$, and therefore serves as a useful tool to assess the achievable estimation performance given the structural dependence of the observations on the PoI [37], here \mathbf{x}_s . When $Q = 1$, localization is infeasible as no coherence dimension remains. Increasing Q sharpens the main lobe and thus improves range resolution (i.e., reduces R_{res}), thereby enhancing localization performance⁸.

The figure also illustrates the information loss incurred by non-coherent processing, which arises from the lack of phase synchronization across the distributed array nodes. Furthermore, note that increasing the subcarrier spacing Δ_f can further improve this resolution⁸ (i.e., reduce R_{res}) without requiring additional observations along q .

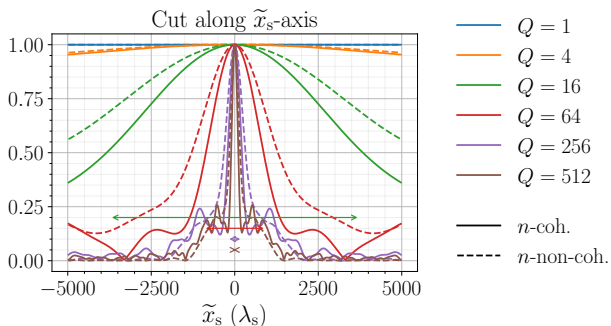


Fig. 10. Normalized coherent and non-coherent AF, $|\text{AF}_{\text{coh}}(\mathbf{0}, \tilde{\mathbf{x}}_s)|$ and $|\text{AF}_{\text{non-coh}}(\mathbf{0}, \tilde{\mathbf{x}}_s)|$, for different values of Q . A one-dimensional cut along $\tilde{\mathbf{x}}_s = \tilde{\mathbf{x}}_s[0]$ is shown. Parameters: $N_g = 400^2$; all other parameters are left at their default values.

Finally, increasing N (Figure 8) or Q (Figure 9) yields stronger localization improvement than increasing D (Figure 7), since additional nodes and subcarriers enrich the steering matrix $\mathbf{A}(\mathbf{x}_s) \in \mathbb{C}^{N \times Q}$ in both the spatial and frequency domains, whereas increasing D (or P) only provides additional observations without adding new structural information.

⁸A sufficiently large N_g was used in the simulations to ensure that the coarse grid captures the main lobe of the objective function. This is enforced by setting $N_g = \max(N_g, \alpha \frac{2R_{\text{scene}}}{R_{\text{res}}})$, where $\alpha \in \mathbb{Z}_+$ is a predefined oversampling factor, set to $\alpha = 4$ in simulation.

V. COMPLEXITY ANALYSIS

This section analyzes the computational complexity of the proposed method against the considered baselines in terms of asymptotic operation counts, illustrating the influence of system parameters on computational requirements. Note that we also highlight operations that can be performed in parallel (i.e., locally at each node rather than at the CPU), and discuss the associated transmission cost, i.e., which quantities need to be forwarded to the CPU.

A. Theoretical Analysis

Table III reports the asymptotic complexity of the processing steps for each method, and for an M -ary constellation, i.e., $\forall q, d \# \mathcal{C}_{\nu(q,d)} = M$. The first two columns correspond to the proposed methods, (16) and (18), without and with the acceleration, respectively. The asymptotic complexity of the localization step is expressed by two terms corresponding to the pilot and data contributions, respectively, each of which must be evaluated across all N_g grid points⁹. Note that the symbol equalization step is independent of the candidate position and needs to be performed only once prior to the localization step. The data contribution is in $\mathcal{O}(N + \sqrt{M})$ (resp. $\mathcal{O}(N + M)$) for MML_{fast} (resp. MML_a) rather than $\mathcal{O}(N\sqrt{M})$ (resp. $\mathcal{O}(NM)$), since the summation over n can be performed independently of the symbol index k (resp. symbol s). Furthermore, the data term additionally requires the computation of $\hat{\gamma}_p(\tilde{\mathbf{x}}_s)$ (13) for all $\tilde{\mathbf{x}}_s$, at a cost of $\mathcal{O}(N_g N Q)$, which merges with the pilot term in the asymptotic complexity. The remaining columns correspond to the baselines introduced above. The SDD approaches share the same complexity as their HDD counterparts, without the hard data decision step.

The following subsections respectively examine acceleration gains, comparison with baselines, and transmission overhead.

1) *Gain of the Acceleration:* As already mentioned, the analytical acceleration MML_{fast} (18) reduces the complexity of the data term from $\mathcal{O}(M)$ in MML_a (16) to $\mathcal{O}(\sqrt{M})$, while yielding the exact same solution, i.e., $\hat{\mathbf{x}}_s^{\text{MML}_a} = \hat{\mathbf{x}}_s^{\text{MML}_{\text{fast}}}$. Therefore, MML_{fast} should always be preferred over MML_a . Note that this reformulation is therefore particularly beneficial for high-data-rate communications using large constellations.

2) *MML_{fast} against baselines:* The cheapest method is the pilot-only approach, as exploiting data payloads for positioning incurs an unavoidable computational cost. Regarding the localization step, the proposed MML_{fast} incurs an additional cost of $\mathcal{O}(N_g Q D (N + \sqrt{M}))$ over PILOT, while HDD methods share the same localization cost as PILOT but incur computational overhead from the symbol equalization step, at a cost of $\mathcal{O}(N Q D)$. Additionally, the DD methods require a one-time data demodulation overhead: $\mathcal{O}(N Q D)$ for soft data estimation, and $\mathcal{O}(M Q D)$ and $\mathcal{O}(N M Q D)$ for centralized and distributed hard decisions, respectively. Note that data demodulation is performed only once in HDD methods,

⁹After grid evaluation, estimates are refined via an optimization algorithm requiring additional objective function evaluations. Since the number of such evaluations depends on the solver strategy rather than on the proposed estimators, it is excluded from the theoretical complexity analysis. In practice, a sufficiently fine search grid yields adequate localization accuracy without refinement.

TABLE III
ASYMPTOTIC COMPUTATIONAL COMPLEXITY PER PROCESSING STEP

Step	MML _a (16)	MML _{fast} (18)	PILOT	GENIE	HDD _{centr}	HDD _{distr}
Channel estimation	—	—	—	—	$\mathcal{O}(NQP)$	$\mathcal{O}(NQP)$
Soft data estimation	—	—	—	—	$\mathcal{O}(NQD)$	$\mathcal{O}(NQD)$
Hard data decision	—	—	—	—	$\mathcal{O}(MQD)$	$\mathcal{O}(NMQD)$
Symbol Equalization i.e., construction of \mathbf{Y}_P , \mathbf{Y} or \mathbf{Y}_{DD}	$\mathcal{O}(NQP)$	$\mathcal{O}(NQP)$	$\mathcal{O}(NQP)$	$\mathcal{O}(NQ(P+D))$	$\mathcal{O}(NQ(P+D))$	$\mathcal{O}(NQ(P+D))$
Localization	$\mathcal{O}(N_g NQ)$ + $\mathcal{O}(N_g QD(N+M))$	$\mathcal{O}(N_g NQ)$ + $\mathcal{O}(N_g QD(N+\sqrt{M}))$	$\mathcal{O}(N_g NQ)$	$\mathcal{O}(N_g NQ)$	$\mathcal{O}(N_g NQ)$	$\mathcal{O}(N_g NQ)$

whereas our approach iterates over the constellation for every position candidate. Consequently, MML_{fast} is cheaper than HDD_{centr} only when $N_g(N + \sqrt{M}) \ll N + M$, and cheaper than HDD_{distr} only when $N_g(N + \sqrt{M}) \ll NM$. The former condition is seldom met in practice, while the latter may be satisfied for small grid sizes, large constellations, and a sufficient number of nodes. Hence, the localization performance gains of the proposed approach over DD baselines are generally achieved at the expense of an increased computational cost.

3) *Transmission Overhead*: In the pilot-only approach (19), pilot symbols \mathbf{S}_P are known at each node, allowing node n to locally compute $\Phi_n^P \triangleq \{\phi_n^P(\tilde{\mathbf{x}}_s)\} \in \mathbb{R}^{N_g}$, i.e., the set of $\phi_n^P(\tilde{\mathbf{x}}_s)$ values evaluated over all candidate grid positions. Each node then transmits Φ_n^P to the CPU, which estimates the UE position as $\arg\max_{\tilde{\mathbf{x}}_s} \sum_n |\phi_n^P(\tilde{\mathbf{x}}_s)|^2$ (see (19)). This results in a transmission of N_g scalars per node. By contrast, MML_{fast} and DD_{centr} (similarly for the soft and hard variants) both require each node to additionally transmit all data observations \mathbf{Y}_D to the CPU—to evaluate the second term of (18) and to collaboratively estimate $\hat{\mathbf{S}}_D$, respectively—resulting in a transmission of QD coefficients per node for the data part. The distributed DD approach reduces this transmission cost: each node n locally produces its own data estimates $\hat{\mathbf{S}}_D[n, q, d] \forall q, d$, computes $\Phi_n^{DD} \triangleq \{\phi_n^{DD}(\tilde{\mathbf{x}}_s)\} \in \mathbb{R}^{N_g}$ (see (21)), and transmits only Φ_n^{DD} to the CPU, i.e., N_g scalars per node. For the considered parameter set, $N_g = 1600 < QD = 4480$, yielding a moderate but tangible reduction in transmission overhead compared to MML_{fast} and DD_{centr}. This transmission reduction is the only advantage of DD_{distr} in this scenario, as its localization performance is inferior, as discussed above.

VI. CONCLUSION

This paper investigates the joint exploitation of pilot and data payloads for source localization where a distributed opportunistic SRX aims to localize the transmitting UE. We develop an MML framework in which both the random channel coefficients at all nodes and the unknown data symbols are treated as NPs, eliminated through marginalization. The optimal solution is derived and shown to be computationally intractable. We then introduce a practical approximation by eliminating the channel dependency in the data term, leveraging pilot-based channel estimates. We further propose a novel closed-form acceleration for QAM modulations, reducing the computational complexity from the full constellation size in $\mathcal{O}(M)$ to its square root $\mathcal{O}(\sqrt{M})$. Through Monte Carlo

simulations, the proposed approach demonstrates superior localization performance against benchmarks from the literature, namely the traditional pilot-only baseline and several DD approaches. It achieves a significant RMSE reduction of up to a factor of 6 over the former, and an SNR gain of up to 4.3 dB over the best DD baseline, for the considered parameter settings. Two key findings further emerge: unlike HDD methods, whose performance degrades with increasing modulation order, the proposed approach remains robust to constellation size and consistently achieves convergence to the GENIE bound at lower SNRs, regardless of the constellation. These results show that marginalizing over the constellation systematically outperforms data demodulation for localization, regardless of the modulation order. This performance improvement comes at the cost of an unavoidable increased computational complexity relative to DD baselines, as discussed in the complexity analysis. Additionally, we study the impact of data demodulation errors on DD-based sensing by jointly considering localization and communication metrics, showing that even imperfect demodulation can still yield localization gains over pilot-only methods. Future work may consider multipath propagation, multistatic radar configurations relying on signal echoes, and extensions to multi-user scenarios, as well as imperfect synchronization and experimental validations.

APPENDIX

A. Proof of Proposition III.1

Proof. Marginalizing over γ yields

$$\mathcal{L}(\mathbf{Y}|\mathbf{S}_D; \tilde{\mathbf{x}}_s) = \mathbb{E}_\gamma \{\mathcal{L}(\mathbf{Y}|\mathbf{S}_D, \gamma; \tilde{\mathbf{x}}_s)\} \quad (28)$$

$$= \int \mathcal{L}(\mathbf{Y}|\mathbf{S}_D, \gamma; \tilde{\mathbf{x}}_s) \mathcal{L}(\gamma) d\gamma. \quad (29)$$

From observation models (3) and (4), the elements of \mathbf{Y} are i.i.d. and follow $\mathbf{Y}[n, q, l] \sim \mathcal{CN}(\gamma[n] \mathbf{A}(\tilde{\mathbf{x}}_s)[n, q] \mathbf{S}[q, l], \sigma_n^2)$. Additionally, we assume $\gamma \sim \mathcal{CN}(\mathbf{0}, \sigma_\gamma^2 \mathbf{I}_N)$. Therefore, the integration in (29) results in

$$\begin{aligned} \mathcal{L}(\mathbf{Y}|\mathbf{S}_D; \tilde{\mathbf{x}}_s) &= \frac{1}{\pi^{K+N} \sigma_n^{2K} \sigma_\gamma^{2N}} \int \prod_n \exp\left(\frac{-1}{\sigma_\gamma^2} |\gamma[n]|^2\right) \\ &\exp\left(-\frac{1}{\sigma_n^2} \sum_{q,l} |\mathbf{Y}[n, q, l] - \gamma[n] \mathbf{A}(\tilde{\mathbf{x}}_s)[n, q] \mathbf{S}[q, l]|^2\right) d\gamma, \end{aligned} \quad (30)$$

where $K = NQL$ is the total number of observations. Since the observations and the channel coefficients are independent across receivers, the integral factorizes as

$$\int f(\mathbf{t})d\mathbf{t} = \int \prod_n f(t_n)dt = \prod_n \int f(t_n)dt_n. \quad (31)$$

Expanding the squared term and moving factors independent of γ outside the integral yields

$$\begin{aligned} \mathcal{L}(\mathcal{Y}|\mathcal{S}_D; \tilde{\mathbf{x}}_s) &= \frac{1}{\pi^{K+N} \sigma_n^{2K} \sigma_\gamma^{2N}} \prod_n \exp\left(\frac{-1}{\sigma_n^2} \sum_{q,l} |\mathcal{Y}[n, q, l]|^2\right) \\ &\int_{\gamma_n} \exp(2\Re\{U_n \gamma_n\} - V |\gamma_n|^2) d\gamma_n, \end{aligned} \quad (32)$$

where

$$U_n \triangleq \frac{1}{\sigma_n^2} \sum_{q,l} \mathcal{Y}^*[n, q, l] \mathbf{A}(\tilde{\mathbf{x}}_s)[n, q] \mathbf{S}[q, l], \quad (33)$$

$$V \triangleq \frac{1}{\sigma_n^2} \sum_{q,l} |\mathbf{S}[q, l]|^2 + \frac{1}{\sigma_\gamma^2}, \quad (34)$$

as $|\mathbf{A}(\tilde{\mathbf{x}}_s)[n, q]|^2 = 1$. Completing the square in the exponent, the remaining integral evaluates to

$$\begin{aligned} &\int_{\gamma_n} \exp(2\Re\{U_n \gamma_n\} - V |\gamma_n|^2) d\gamma_n \\ &= \int_{\gamma_n} \exp\left(-V \left|\frac{U_n^*}{V} - \gamma_n\right|^2 + \frac{|U_n|^2}{V}\right) d\gamma_n \end{aligned} \quad (35)$$

$$= \exp\left(\frac{|U_n|^2}{V}\right) \frac{\pi}{V}, \quad (36)$$

where we used the property $\int_z e^{-\alpha|z|^2} dz = \pi/\alpha$. Substituting (36) along with the expressions of U_n and V back into (32) leads to

$$\begin{aligned} \mathcal{L}(\mathcal{Y}|\mathcal{S}_D; \tilde{\mathbf{x}}_s) &= \frac{1}{\pi^{K+N} \sigma_n^{2K} \sigma_\gamma^{2N}} \\ &\prod_n \exp\left(\frac{-1}{\sigma_n^2} \sum_{q,l} |\mathcal{Y}[n, q, l]|^2\right) \frac{\pi}{\frac{1}{\sigma_n^2} \sum_{q,l} |\mathbf{S}[q, l]|^2 + \frac{1}{\sigma_\gamma^2}} \\ &\times \exp\left(\frac{\left|\frac{1}{\sigma_n^2} \sum_{q,l} \mathcal{Y}^*[n, q, l] \mathbf{A}(\tilde{\mathbf{x}}_s)[n, q] \mathbf{S}[q, l]\right|^2}{\frac{1}{\sigma_n^2} \sum_{q,l} |\mathbf{S}[q, l]|^2 + \frac{1}{\sigma_\gamma^2}}}\right), \end{aligned} \quad (37)$$

where the gray terms are independent of $\tilde{\mathbf{x}}_s$ and \mathcal{S} and can thus be absorbed into a multiplicative constant C , given by

$$C = \frac{\exp\left(-\|\mathcal{Y}\|_F^2 / \sigma_n^2\right)}{\pi^{K+N-1} \sigma_n^{2K} \sigma_\gamma^{2N}}. \quad (38)$$

It remains to compute $\mathcal{L}(\mathcal{Y}_P, \mathcal{Y}_D; \tilde{\mathbf{x}}_s) = \mathbb{E}_{\mathcal{S}_D} \{\mathcal{L}(\mathcal{Y}_P, \mathcal{Y}_D|\mathcal{S}_D; \tilde{\mathbf{x}}_s)\}$. Since the summations over q and l appear inside the squared norm (i.e., frequency and time coherence are preserved), the sums cannot be factorized. Consequently, one must exhaustively enumerate all possible symbol combinations $\mathcal{S}_D \in \mathcal{C}_\nu^{Q \times D}$, yielding

$$\mathcal{L}(\mathcal{Y}_P, \mathcal{Y}_D; \tilde{\mathbf{x}}_s) = \sum_{\mathcal{S}_D \in \mathcal{C}_\nu^{Q \times D}} \mathcal{L}(\mathcal{Y}|\mathcal{S}_D; \tilde{\mathbf{x}}_s) \mathcal{L}(\mathcal{S}_D), \quad (39)$$

which concludes the proof. \square

B. Proof of Proposition III.2

Proof. The pilot term follows directly from Proposition III.1 by restricting to the known pilot sequence \mathcal{S}_P rather than the entire frame \mathcal{S} , discarding constant terms, denoting $\mathcal{P}_P \triangleq \|\mathcal{S}_P\|_F^2$ and substituting (14). Assuming a uniform distribution over the constellations, the data term is computed as

$$\begin{aligned} &\mathbb{E}_{\mathcal{S}_D} \{\mathcal{L}(\mathcal{Y}_D|\mathcal{S}_D; \tilde{\mathbf{x}}_s, \hat{\gamma}_p(\tilde{\mathbf{x}}_s))\} \\ &= \int_{\mathcal{S}_D} \prod_{n,q,d} \mathcal{L}(\mathcal{Y}_D[n, q, d]|\mathcal{S}_D; \tilde{\mathbf{x}}_s, \hat{\gamma}_p(\tilde{\mathbf{x}}_s)) \mathcal{L}(\mathcal{S}_D) d\mathcal{S}_D \quad (40) \\ &= \prod_{q,d} \sum_{s \in \mathcal{C}_{\nu(q,d)}} \prod_n \mathcal{L}(\mathcal{Y}_D[n, q, d]|\mathcal{S}_D; \tilde{\mathbf{x}}_s, \hat{\gamma}_p(\tilde{\mathbf{x}}_s)) \frac{1}{\#\mathcal{C}_{\nu(q,d)}}, \end{aligned} \quad (41)$$

where (40) leverages the independence of the observations, and (41) exploits the property given in (31), accounting for the discrete nature of the symbols. The likelihood in (41) is given by

$$\begin{aligned} &\mathcal{L}(\mathcal{Y}_D[n, q, d]|\mathcal{S}_D; \tilde{\mathbf{x}}_s, \hat{\gamma}_p(\tilde{\mathbf{x}}_s)) \\ &= \frac{1}{\pi \sigma_n^2} \exp\left(\frac{-1}{\sigma_n^2} |\mathcal{Y}_D[n, q, d] - \hat{\gamma}_p(\tilde{\mathbf{x}}_s)[n] \mathbf{A}(\tilde{\mathbf{x}}_s)[n, q] s|^2\right). \end{aligned} \quad (42)$$

Substituting (42) into (41), expanding the squared norm, taking the logarithm of (10), and omitting constant terms yields (16), which completes the proof. \square

C. Proof of Proposition III.3

Proof. Let us define $H_q(\tilde{\mathbf{x}}_s) \triangleq \sum_{n=0}^{N-1} |\widehat{\mathbf{H}}_p(\tilde{\mathbf{x}}_s)[n, q]|^2$ and $S_{qd}^*(\tilde{\mathbf{x}}_s) \triangleq \sum_{n=0}^{N-1} \mathcal{Y}_D^*[n, q, d] \widehat{\mathbf{H}}_p(\tilde{\mathbf{x}}_s)[n, q]$. For a M_{qd} -QAM constellation, the data term likelihood (inside the log) in (16) can be rewritten as

$$\begin{aligned} \mathbb{S} &\triangleq \sum_{s \in \mathcal{C}_{\nu(q,d)}} \exp\left(\frac{2}{\sigma_n^2} \Re\{S_{qd}^*(\tilde{\mathbf{x}}_s) s\} - \frac{1}{\sigma_n^2} H_q(\tilde{\mathbf{x}}_s) |s|^2\right) \\ &= \sum_{r,i} \exp\left(\frac{1}{\sigma_n^2} \left(2\Re\{S_{qd}^*(\tilde{\mathbf{x}}_s) s_{r,i}\} - H_q(\tilde{\mathbf{x}}_s) |s_{r,i}|^2\right)\right), \end{aligned} \quad (43)$$

where $s_{r,i}$ is given by (17) and $0 \leq r, i \in \mathbb{Z} \leq \sqrt{M_{qd}} - 1$. The remainder of the proof proceeds as follows. First, (17) is substituted into (43), and the real part and squared magnitude of the products involving $s_{r,i}$ with $S_{qd}^*(\tilde{\mathbf{x}}_s)$ and $H_q(\tilde{\mathbf{x}}_s)$ are expanded using the identities $\Re\{z_1 z_2\} = \Re\{z_1\} \Re\{z_2\} - \Im\{z_1\} \Im\{z_2\}$ and $|z_1|^2 = (\Re\{z_1\})^2 + (\Im\{z_1\})^2$, $\forall z_1, z_2 \in \mathbb{C}$. The real and imaginary contributions are then separated, yielding a product of a sum over r and a sum over i . Finally, the summation indices are reparametrized as $r' = 2r - \sqrt{M} + 1$, with r' ranging over odd integers in $[-\sqrt{M} + 1, \sqrt{M} - 1]$ (and

similarly for i'). These steps yield the following intermediate result:

$$S = \prod_{\tilde{\mathfrak{R}} \in \{\mathfrak{R}, \mathfrak{I}\}} \left[\sum_{\substack{k=-\sqrt{M}-1 \\ k \text{ odd}}}^{\sqrt{M}-1} \exp \left(\frac{1}{\sigma_n^2} 2\tilde{\mathfrak{I}} \{S_{qd}^* (\tilde{\mathbf{x}}_s)\} \frac{k}{\sqrt{\mathcal{E}_{M_{qd}}}} \right) \exp \left(-\frac{1}{\sigma_n^2} \text{H}_q \frac{k^2}{\mathcal{E}_{M_{qd}}} \right) \right], \quad (44)$$

where k is the running index replacing r' and i' . The symmetric pairs $(-k, k)$, corresponding to constellation points of equal amplitude (see Figure 3), are then grouped together, enabling the use of the hyperbolic cosine identity. Taking the logarithm of the resulting expression completes the proof. \square

REFERENCES

- [1] K. Meng, C. Masouros, A. P. Petropulu, and L. Hanzo, "Cooperative ISAC Networks: Opportunities and Challenges," *IEEE Wireless Commun.*, pp. 1–8, 2024.
- [2] L. Zheng, M. Lops, Y. C. Eldar, and X. Wang, "Radar and Communication Coexistence: An Overview: A Review of Recent Methods," *IEEE Signal Process. Mag.*, vol. 36, no. 5, pp. 85–99, Sep. 2019.
- [3] S. Mazahir, S. Ahmed, and M.-S. Alouini, "A Survey on Joint Communication-Radar Systems," *Front. Comms. Net.*, vol. 1, p. 619483, Feb. 2021.
- [4] F. Liu, C. Masouros, A. P. Petropulu, H. Griffiths, and L. Hanzo, "Joint Radar and Communication Design: Applications, State-of-the-Art, and the Road Ahead," *IEEE Trans. Commun.*, vol. 68, no. 6, pp. 3834–3862, Jun. 2020.
- [5] Z. Feng, Z. Fang, Z. Wei, X. Chen, Z. Quan, and D. Ji, "Joint radar and communication: A survey," *China Commun.*, vol. 17, no. 1, pp. 1–27, Jan. 2020.
- [6] J. A. Zhang, F. Liu, C. Masouros, R. W. Heath, Z. Feng, L. Zheng, and A. Petropulu, "An Overview of Signal Processing Techniques for Joint Communication and Radar Sensing," *IEEE J. Sel. Top. Signal Process.*, vol. 15, no. 6, pp. 1295–1315, Nov. 2021.
- [7] S. Lu, F. Liu, Y. Xiong, Z. Du, Y. Cui, S. Li, W. Yuan, J. Yang, and S. Jin, "Sensing With Random Communication Signals," Apr. 2025.
- [8] Z. Wei, Y. Wang, L. Ma, S. Yang, Z. Feng, C. Pan, Q. Zhang, Y. Wang, H. Wu, and P. Zhang, "5G PRS-Based Sensing: A Sensing Reference Signal Approach for Joint Sensing and Communication System," *IEEE Trans. Veh. Technol.*, vol. 72, no. 3, pp. 3250–3263, Mar. 2023.
- [9] M. Golzadeh, E. Tirola, J. Talvitie, L. Anttila, K. Hooli, O. Tervo, and M. Valkama, "Joint Sensing and UE Positioning in 5G-6G: PRS Range Estimation with Suppressed Ambiguity," in *2024 IEEE Radar Conference (RadarConf24)*. IEEE, May 2024, pp. 1–6.
- [10] Z. Wei, F. Li, H. Liu, X. Chen, H. Wu, K. Han, and Z. Feng, "Multiple Reference Signals Collaborative Sensing for Integrated Sensing and Communication System Towards 5G-A and 6G," *IEEE Trans. Veh. Technol.*, vol. 73, no. 10, pp. 15185–15199, Oct. 2024.
- [11] 3GPP, "5G; NR; Physical channels and modulation (3GPP TS 38.211 version 19.1.0 Release 19)," 3GPP, Tech. Rep. TS 138 211, Oct. 2025.
- [12] F. Liu, Y. Zhang, Y. Xiong, S. Li, W. Yuan, F. Gao, S. Jin, and G. Caire, "CP-OFDM Achieves the Lowest Average Ranging Sidelobe Under QAM/PSK Constellations," *IEEE Trans. Inform. Theory*, vol. 71, no. 9, pp. 6950–6967, Sep. 2025.
- [13] M. F. Keskin, M. M. Mojahedian, J. O. Lacruz, C. Marcus, O. Eriksson, A. Giorgetti, J. Widmer, and H. Wymeersch, "Fundamental Trade-Offs in Monostatic ISAC: A Holistic Investigation Toward 6G," *IEEE Trans. Wireless Commun.*, vol. 24, no. 9, pp. 7856–7873, Sep. 2025.
- [14] Z. Du, F. Liu, Y. Xiong, T. X. Han, Y. C. Eldar, and S. Jin, "Reshaping the ISAC Tradeoff Under OFDM Signaling: A Probabilistic Constellation Shaping Approach," *IEEE Trans. Signal Process.*, vol. 72, pp. 4782–4797, 2024.
- [15] M. Wypich and T. P. Zielinski, "OFDM-Based Passive Radar Using Reference Signals and User Data," in *2025 IEEE Radar Conference (RadarConf25)*. Krakow, Poland: IEEE, Oct. 2025, pp. 847–852.
- [16] —, "Experimental Evaluation of 5G NR OFDM-Based Passive Radar Exploiting Reference, Control, and User Data," *Sensors*, vol. 26, no. 4, p. 1317, Feb. 2026.
- [17] D. Brunner, L. Giroto De Oliveira, C. Muth, S. Mandelli, M. Henninger, A. Diewald, Y. Li, M. Basim Alabd, L. Schmalen, T. Zwick, and B. Nuss, "Bistatic OFDM-Based ISAC With Over-the-Air Synchronization: System Concept and Performance Analysis," *IEEE Trans. Microwave Theory Techn.*, vol. 73, no. 5, pp. 3016–3029, May 2025.
- [18] M. Henninger, L. Giroto, A. Elkelesh, and S. Mandelli, "Hybrid Resource Allocation Scheme for Bistatic ISAC with Data Channels," Jan. 2026, arXiv:2601.11110 [eess].
- [19] N. Zhao, Q. Chang, X. Shen, Y. Wang, and Y. Shen, "Joint Target Localization and Data Detection in Bistatic ISAC Networks," *IEEE Trans. Commun.*, pp. 1–1, 2024.
- [20] M. F. Keskin, S. Mura, M. Mizmizi, D. Tagliaferri, and H. Wymeersch, "Bridging the Gap via Data-Aided Sensing: Can Bistatic ISAC Converge to Genie Performance?" in *2025 IEEE Radar Conference (RadarConf25)*. Krakow, Poland: IEEE, Oct. 2025, pp. 514–519.
- [21] J. O. Berger, B. Liseo, and R. L. Wolpert, "Integrated Likelihood Methods for Eliminating Nuisance Parameters," *Statistical Science*, vol. 14, no. 1, pp. 1–28, Feb. 1999.
- [22] C. Mensing, S. Sand, A. Dammann, and W. Utschick, "Data-Aided Location Estimation in Cellular OFDM Communications Systems," in *GLOBECOM 2009 - 2009 IEEE Global Telecommunications Conference*. Honolulu, Hawaii: IEEE, Nov. 2009, pp. 1–7.
- [23] A. Gupta, P. Ganji, S. Srivastava, and A. K. Jagannatham, "Data-Aided Bistatic Sensing and Communication for mmWave MIMO-OFDM ISAC Systems," *IEEE Trans. Commun.*, pp. 1–1, 2025.
- [24] S. Monfared, T.-H. Nguyen, T. Van Der Vorst, P. De Doncker, and F. Horlin, "Iterative NDA Positioning Using Angle-of-Arrival Measurements for IoT Sensor Networks," *IEEE Trans. Veh. Technol.*, vol. 69, no. 10, pp. 11369–11382, Oct. 2020.
- [25] A. M. Graff and T. E. Humphreys, "OFDM-Based Positioning With Unknown Data Payloads: Bounds and Applications to LEO PNT," *IEEE Trans. Wireless Commun.*, vol. 25, pp. 7505–7519, 2026.
- [26] M. Reniers, M. Willame, J. Louveaux, and L. Vandendorpe, "Joint Pilot and Unknown Data-based Localization for OFDM Opportunistic Radar Systems," Jan. 2026, arXiv:2601.15785 [eess].
- [27] A. Sakhnini, S. De Bast, M. Guenach, A. Bourdoux, H. Sahli, and S. Pollin, "Near-Field Coherent Radar Sensing Using a Massive MIMO Communication Testbed," *IEEE Trans. Wireless Commun.*, vol. 21, no. 8, pp. 6256–6270, Aug. 2022.
- [28] J. A. Nanzer, S. R. Mghabghab, S. M. Ellison, and A. Schlegel, "Distributed Phased Arrays: Challenges and Recent Advances," *IEEE Trans. Microwave Theory Techn.*, vol. 69, no. 11, pp. 4893–4907, Nov. 2021.
- [29] M. Rashid and J. A. Nanzer, "Frequency and Phase Synchronization in Distributed Antenna Arrays Based on Consensus Averaging and Kalman Filtering," *IEEE Trans. Wireless Commun.*, vol. 22, no. 4, pp. 2789–2803, Apr. 2023.
- [30] D. Pauluzzi and N. Beaulieu, "A comparison of SNR estimation techniques for the AWGN channel," *IEEE Trans. Commun.*, vol. 48, no. 10, pp. 1681–1691, Oct. 2000.
- [31] S. Boumard, "Novel noise variance and SNR estimation algorithm for wireless MIMO OFDM systems," in *GLOBECOM '03. IEEE Global Telecommunications Conference (IEEE Cat. No.03CH37489)*. San Francisco, CA, USA: IEEE, 2003, pp. 1330–1334.
- [32] W.-C. Huang, C.-P. Li, and H.-J. Li, "An investigation into the noise variance and the SNR estimators in imperfectly-synchronized OFDM systems," *IEEE Trans. Wireless Commun.*, vol. 9, no. 3, pp. 1159–1167, Mar. 2010.
- [33] K. Koor, Y. Qiu, L. C. Kwek, and P. Rebentrost, "A short tutorial on Wirtinger Calculus with applications in quantum information," 2023, arXiv:2312.04858 [quant-ph].
- [34] J. A. Nelder and R. Mead, "A Simplex Method for Function Minimization," *The Computer Journal*, vol. 7, no. 4, pp. 308–313, Jan. 1965.
- [35] J. Gutierrez-Meana, J. A., and F. Las-Heras, "High Frequency Techniques: the Physical Optics Approximation and the Modified Equivalent Current Approximation (MECA)," in *Electromagnetic Waves Propagation in Complex Matter*, A. Kishk, Ed. InTech, Jun. 2011.
- [36] G. A. Baduge, M. Vaezi, J. K. Dassanayake, M. Z. Hameed, E. Ollila, and S. A. Vorobyov, "Frequency Range 3 for ISAC in 6G: Potentials and Challenges," Jun. 2025, arXiv:2506.18243 [cs].
- [37] G. Monnoyer, L. Defraigne, B. Sambon, J. Louveaux, and L. Vandendorpe, "Chirp-Based Aliasing Analysis of Arrays in the Spherical Wavefront Regime," in *2025 IEEE 26th International Workshop on Signal Processing and Artificial Intelligence for Wireless Communications (SPAWC)*. Surrey, United Kingdom: IEEE, Jul. 2025, pp. 1–5.